01 Jul 2013

Wind-Induced Torsion Vibration of the Super High-Rise Building of Shenzhen Energy Center

Feng Ruo-Qiang

Ye Jihong

Guirong Yan
Missouri University of Science and Technology, yang@mst.edu

Li Qing-Xiang

et. al. For a complete list of authors, see https://scholarsmine.mst.edu/civarc_enveng_facwork/2466

Recommended Citation

F. Ruo-Qiang et al., "Wind-Induced Torsion Vibration of the Super High-Rise Building of Shenzhen Energy Center," *Structural Design of Tall and Special Buildings*, vol. 22, no. 10, pp. 802 - 815, Wiley, Jul 2013.
The definitive version is available at https://doi.org/10.1002/tal.749

THE STRUCTURAL DESIGN OF TALL AND SPECIAL BUILDINGS
Struct. Design Tall Spec. Build. **22**, 802–815 (2013)
Published online 5 December 2011 in Wiley Online Library (wileyonlinelibrary.com). DOI: 10.1002/tal.749

Wind-induced torsion vibration of the super high-rise building of Shenzhen Energy Center

Feng Ruo-qiang[1]*,†, Ye Jihong[1], Guirong Yan[2], Li Qing-xiang[3] and Yao Bin[1]

[1]*The Key Laboratory of Concrete and Prestressed Concrete Structures of Ministry of Education, Southeast University, NanJing 210096, China*
[2]*School of engineering, University of Western Sydney, Penrith, NSW 1797, Australia*
[3]*Guangdong Provincial Academy of Building Research, Guangzhou 510500, China*

SUMMARY

The synchronous multipoint scanning system technique in wind tunnel tests and random vibration theory method were used to analyze the wind-induced torsion vibration of some irregularly shaped super high-rise buildings in downtowns. The torsion vibration modes and the spectra of torsion wind load were studied, and the proportions of mean wind torsion, inertia torsion and the mass eccentricity torsion caused by horizontal inertia forces are discussed. The following conclusions can be drawn. First, the third and fourth modes have torsion vibration shapes, and their frequencies are in the high-energy area of the spectra of the torsion wind load; the third and fourth modes are included in the resonant component of the spectra of the top torsion angle of the building, and the third mode is dominant. Second, the torsion stiffness is weak in the high stories of the building, so the inertia torsion is dominant, whereas the torsion stiffness is strong in the low stories; the mean wind torsion is dominant. The proportion of the mass eccentricity torsion moment caused by horizontal inertia forces is small. Finally, the wind-induced torsion moment at a 90° wind angle is the largest, whereas the torsion eccentricity is 46% of the radius of gyration and is much greater than the mass eccentricity; thus, the wind-induced torsion should be considered. The wind-induced torsion vibration of the building is sensitive to wind directions. Copyright © 2011 John Wiley & Sons, Ltd.

Received 22 August 2011; Accepted 3 November 2011

KEYWORDS: super high-rise building; wind tunnel test; torsion vibration; torsion eccentricity

1. INTRODUCTION

With the rapid development of China's economy, more super-high buildings have been built in the coastal areas of China (Council on Tall Buildings, Structural Branch, Architectural Society of China, 2010). The heights of these high buildings are greater than 150 m, and they generally have flexible and low-damping characteristics. They are susceptible to vibration problems due to wind loads. Consequently, vibration mitigation has attracted much interest from a practical point of view (Irwin, 2009). The wind-induced excitations of super-high buildings have the potential to reduce their structural safety and cause discomfort to the occupants of the building (Kareem, 1983). Modern super high-rise buildings tend to be more sensitive to wind-induced torsional excitation because more complex building shapes and adopted structural systems often accentuate both structural and aerodynamic eccentricities, especially when the first torsion natural vibration frequency is near the first two-sway modes of the vibration frequency. Moreover, modern super high-rise buildings are also often built in groups, which creates a complex flow field around the building group and induces larger torsion moments on the buildings (Lam *et al*., 2011). The torsion vibration may increase the acceleration of the rooms that are near the edges of the buildings, which may cause discomfort to building occupants.

*Correspondence to: Feng Ruo-qiang, Office 407, Building of Civil Engineering Campus of Si Pailou Nanjing, Jiangsu province 210096, People's Republic of China.
†E-mail: hitfeng@163.com

Therefore, it is of considerable interest to study the torsional response of structurally asymmetric buildings (eccentricity between stiffness and mass centers) (Zhang *et al*., 1995).

Tallin and Ellingwood (1985), Kareem (1985) and Islam *et al*. (1990) theoretically investigated the torsional response or coupled lateral–torsional response of wind-excited isolated eccentric buildings in terms of simplified wind force models. Their results indicate that the total response of an eccentric building could be significantly underestimated if the torsional response is not included in the analysis. The spectra of the torsional dynamic loads of tall buildings were studied using a wind tunnel in a paper by Lina *et al*. (2005).

It has been recognized that for many high-rise buildings, the crosswind and torsional responses may exceed the alongwind response in terms of both limit state and serviceability designs (Kareem, 1985). Nevertheless, most existing codes and standards (e.g. (American Society of Civil Engineers (ASCE), 2006; China National Standard, 2006)) only provide procedures for the alongwind response because of the complexity of the crosswind and torsional responses.

The Shenzhen Energy Center mansion, which possesses an irregular shape, was selected to analyze the wind-induced torsion vibration, as shown in Figure 1. The height of the building is 222 m, and the number of stories is 43—one underground story and 42 aboveground stories, with stories one through eight acting as podiums. A reinforced concrete structure system was adopted in the mansions construction, and the damping ratio is 5%. The design wind pressure at a height of 10 m with a hundred-year return period is 0.9 kPa. The average size of the building is 55.6 m $\times$ 34 m. The terrain of the buildings is classified as being category C, in accordance with the Chinese load code (China National Standard, 2006). The exponent of the mean wind profiles for the terrain category C is 0.22, and the corresponding gradient height is 400 m.

The high-frequency force-balance (HFFB) technique has been used to determine the wind-induced response of many high-rise buildings since its development around 1980 (Tschanz and Davenport, 1983), and it has become the customary method for the aerodynamic characterization of tall buildings. It has gained popularity for two main reasons: its relatively low test cost and its ability to provide engineers with design information at an early design stage of a project. The basis of the technique is the estimation of the modal forces from the overturning and torsional moments measured at the base of a building model using an appropriate balance. Such an approach has, however, some major limitations:

- The results are only valid for buildings with linear sway mode shapes, and analytical corrections are required for buildings with sway mode shapes that vary significantly from being linear.
- Only the fundamental modes of vibration in the two-sway and one-torsional modes are included in the response computation; higher-mode effects are neglected.
- The effects of the cross-correlation of the wind forces on the modal forces are neglected.
- It is nearly impossible to estimate the full details of the modal forces for coupled 3-D and complex modes.

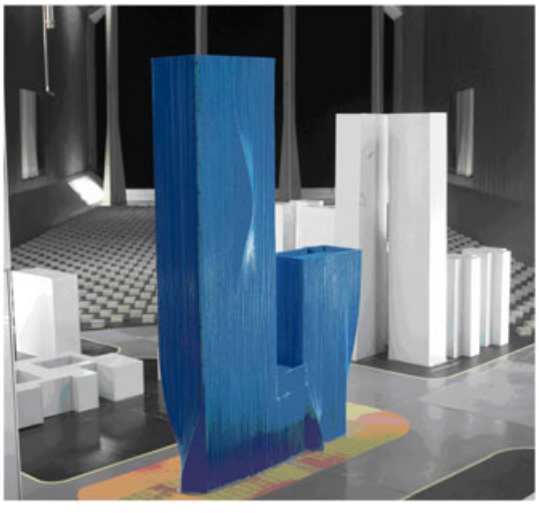

Figure 1. Model of the super high-rise building.

DOI: 10.1002/tal

This is due not only to its technical simplicity but also to the fact that it overcomes some technical difficulties inherent to the synchronous multipoint scanning system (SMPSS) technique in estimating the wind pressure field of a building through experimental wind tunnel tests.

For flexible super high-rise buildings with complex shapes and coupled 3-D modes, all of the other limitations may also significantly influence the accuracy of the conventional prediction approach (Yip and Flay, 1995).

The external wind pressure field may be directly estimated through the SMPSS technique on rigid scaled models. The SMPSS technique implies a series of experimental measurements, which involve some technical difficulties. These are essentially due to the large number of pressure taps that are needed to adequately define the integrated wind load (in theory, an infinite number). However, the limit on the number of pressure taps needed within the SMPSS technique makes it difficult to obtain representative pressure measurements for structural design precisely (Ruo-qiang, 2008). Nevertheless, with a sufficient number of pressure taps, the base moments and shear force obtained with the HFFB and the SMPSS are in good agreement (Cluni *et al*., 2011). Moreover, with the development of equipment in the wind tunnel laboratory of Guangdong Provincial Academy of Building Research, the external pressure field can be characterized by 512 simultaneously measured pressure taps, which can generally satisfy the requirements for estimating the simultaneous wind pressure field on super high-rise buildings. With methods of random vibration theory and spectral analysis (Simiu and Scanlan, 1996; Holmes, 2001), the wind-induced responses of super-tall buildings can be determined. Because the limitations of HFFB can be overcome using the method of random vibration theory combined with the SMPSS technique, the wind-induced responses of super high-rise buildings are more precise than those of HFFB.

2. WIND-INDUCED TORSION MOMENT OF SUPER HIGH-RISE BUILDINGS

A structural floor model was used to analyze the wind-induced response of super high-rise buildings. It was assumed that the stiffness in the plane of the floor slab is infinite, and the degrees of freedom can be simplified to three: two horizontal translational degrees of freedom and one torsion degree of freedom around the vertical direction.

According to the mechanism of the wind torsion moment, three parts were included. The first part is the torsion moment of the mean wind load caused by the irregular shape of the building and the wind interference effects observed downtown.

The second part is the wind-induced torsion vibration of the building. When the shape of a building varies significantly along the height and the first torsion natural vibration frequency is near the first two-sway modes of vibration frequency, the wind-induced torsion vibration is greater.

The third part is caused by the eccentricity between the stiffness center and mass center. Because the inertia force acts on the mass center of the building and when there is an eccentricity between the stiffness center and mass center, the torsion moment is caused by the horizontal inertia force.

The total torsion moment was the vectorial sum of the three abovementioned parts of the torsion moment. The noncoincidence of the mass center and the stiffness center leads to a coupled vibration of the torsion vibration mode shape and sway vibration mode shape. Because the eccentricity between the stiffness center and mass center of the building was less than 10% of the width of the building section, the couple vibration of torsion vibration mode shape and sway vibration mode shape did not need to be considered (Shuguo, 1998; Cai *et al*., 2007).

The aforementioned three parts of the torsion moment were calculated in this paper, and the wind-induced torsion vibration and the torsion moment caused by the eccentricity of the mass center were studied.

3. NATURAL FREQUENCIES OF SHENZHEN ENERGY CENTER MANSION

The *y*-direction-direction sway vibration is dominant in the first mode of the building, and the *x*-direction sway vibration is dominant in the second mode; torsion vibration is dominant in the third mode. Whether the mode is a torsion dominant mode or a sway movement dominant mode can be determined by the rotation direction factor D_j, as shown in Equation (1).

DOI: 10.1002/tal

$$D_j = \frac{\theta_j M_\theta \theta_j^{'}}{\left(\varphi_{xj} M \varphi^{'}_{xy} + \theta_j M \theta^{'}_j + \varphi_{yj} M \varphi^{'}_{yj}\right)} \tag{1}$$

where M is the translational mass; M_θ is the moment of inertia, $M_{i\theta} = M_i r^2$; M_i is the mass of story i; r is the rotation radius of story i; and ϕ_{xj}, ϕ_{yj} and θ_j are the x-direction components, y-direction components and rotation component of vibration shape of mode j, respectively.

When the rotation direction factor of the mode is 1, the torsion vibration is dominant and there is no translational movement; when the rotation direction factor of the mode is 0, the sway vibration is dominant and there is no torsion vibration; when the rotation direction factor of the mode is greater than 0.5, the torsion vibration is dominant; when the rotation direction factor of the mode is less than 0.5, the translational movement is dominant. The first 14 vibration modes are listed in Table 1. As shown in Table 1, the torsion vibration is dominant in the 3rd, 7th, 8th, 9th and 13th modes; the translational movement is dominant in the 1st, 2nd, 4th, 6th, 10th, 12th and 14th modes, though they have torsion components. The frequency of the third torsion mode is near that of the first two-sway modes.

4. WIND TUNNEL TESTS OF SUPER HIGH-RISE BUILDINGS

Information regarding the fluctuating wind load of the buildings was obtained through wind tunnel tests on a rigid wind-pressure model. The time histories of wind pressure exerted on the buildings were simultaneously acquired at a rate of 313 Hz through an electronically scanned pressure system. The wind tunnel test models of the buildings are shown in Figure 2. The length scale of the building in the wind tunnel tests was 1/300. The terrain category of buildings was C, in accordance with the Chinese load code (China National Standard, 2006). The wind direction and the structural coordinate system are shown in Figure 3, and the wind angle was 0°–360°; 24 wind angles were adopted, and the interval of each angle was 15°. The exponent of the mean wind profiles for the terrain category C is 0.22, and the corresponding gradient wind height is 400 m. The wind characteristics were achieved by a combination of turbulence-generating spires, a barrier at the entrance of the wind tunnel and roughness elements along the wind tunnel floor upstream of the model. Figure 4 shows the simulated mean wind-speed profiles and the longitudinal component profiles of turbulence intensities, and Figure 5 shows the atmospheric turbulence power spectra for the terrain category C.

The concentrated wind forces acting on the stories of the building were the horizontal x-direction force F_x, the horizontal y-direction force F_y and the torsion moment M_z. The directions of F_x, F_y and M_z are shown in Figure 3 and are expressed in Equations (2)–(4).

$$F_{jx} = \sum_{i=1}^{n} P_{ri}(t)(\cos\alpha_i) L_i \tag{2}$$

$$F_{jy} = \sum_{i=1}^{n} P_{ri}(t)(\sin\alpha_i) L_i \tag{3}$$

Table 1. Natural frequencies and modal rotation direction factors of Shenzhen Energy Center mansion.

Mode	1	2	3	4	5	6	7
Frequency (Hz)	0.186	0.254	0.317	0.402	0.661	0.707	0.818
Rotation direction factor	0	0	0.88	0.19	0.04	0.11	0.68
Mode	8	9	10	11	12	13	14
Frequency (Hz)	0.888	0.938	1.362	1.479	1.531	1.779	1.996
Rotation direction factor	0.61	0.54	0.22	0.18	0.15	0.78	0.12

DOI: 10.1002/tal

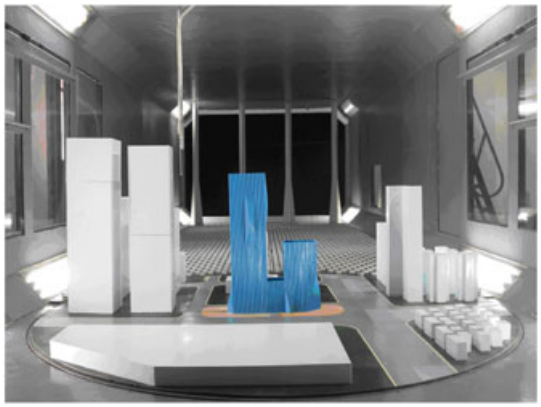

Figure 2. Wind tunnel test of super high-rise building.

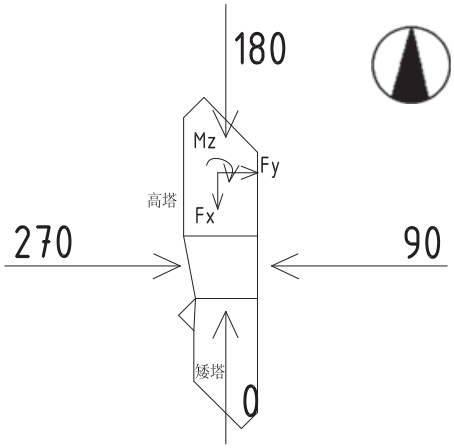

Figure 3. Wind direction of Shenzhen Energy Center mansion.

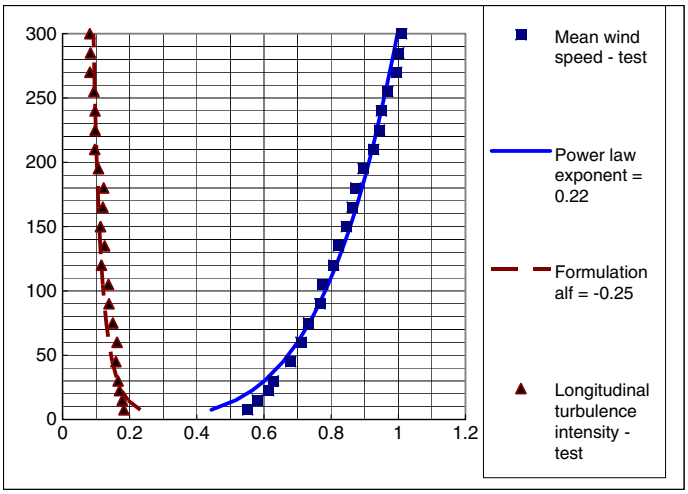

Figure 4. Profile of the mean longitudinal wind velocities and turbulence intensities.

DOI: 10.1002/tal

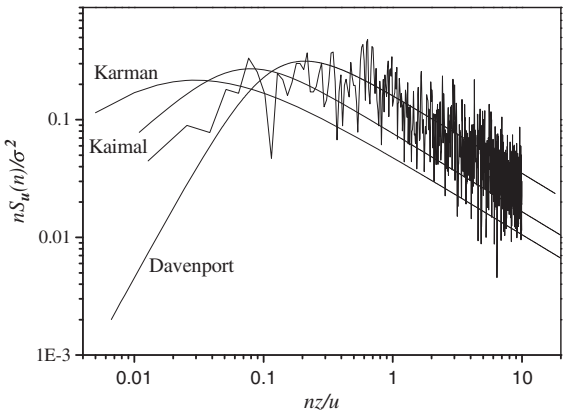

Figure 5. Atmospheric turbulence spectra.

$$M_{jz} = \sum_{i=1}^{n} P_{ri}(t)(\sin\alpha_i)L_i \times x_i + \sum_{i=1}^{n} P_{ri}(t)(\cos\alpha_i)L_i \times y_i \tag{4}$$

where α_i is the angle between the normal direction of the measured pressure tap i and x-direction; L_i is the width of the measured pressure tap i; n is the number of measured pressure taps in story j; x_i and y_i are the distances between tap i and the stiffness center of story j. The units of F_x, F_y and M_z are kN/m, kN/m and kN.m/m, respectively, which correspond to concentrated forces per meter.

5. COMPUTATION OF THE WIND-INDUCED TORSION RESPONSE OF SUPER HIGH-RISE BUILDINGS

5.1. Computation of the wind-induced response of super high-rise buildings

With the application of SMPSS technique in tunnel tests, the time history of wind pressures of the measured pressure taps were obtained, and the measured wind forces were applied on each story of the building. Moreover, the time histories of wind forces were transferred to the fluctuating wind load spectra. With the fluctuating wind load spectra, random vibration theory was used to calculate the wind-induced response of the building.

Assuming that the wind forces are stationary Gaussian random loads, the spectral density matrix of the displacement response of the wind-induced coupled motion can be computed in matrix notation from

$$S(x,y,z,n) = \sum_{j=1}^{m} S_j(x,y,z,n) = \sum_{j=1}^{m}\sum_{k=1}^{m} \varphi_j(x,y,z)\varphi_k\left(x',y',z'\right)H_j(in)H_k(-in)S_{F_jF_k}(x,y,z,n) \tag{5}$$

where (x, y, z) and (x', y', z') are dummy space variables, n is the frequency in Hz, m is the number of modes included, $H_j(in)$ is the frequency response function of mode j, $\varphi_j(x, y, z)$ is the 3-D vibration shape of mode j, and $S_{F_jF_k}(x, y, z, n)$ are the spectral densities of the generalized wind forces.

DOI: 10.1002/tal

The covariance of the top displacement and acceleration response of mode j is

$$\sigma_j(x,y,z) = \left[\int_0^\infty S_j(x,y,z,n)dn\right]^{1/2}$$
$$\sigma_{aj}(x,y,z) = \left[\int_0^\infty S_j(x,y,z,n)\omega_j^4 dn\right]^{1/2} \tag{6}$$

The combination of the modal displacement and acceleration responses with the completely quadratic combination method produces the following:

$$\sigma(x,y,z) = \sqrt{\sum_j^r\sum_i^k \sigma_{ij}^2\varphi_i(x,y,z)\varphi_j(x',y',z')}$$
$$\sigma_a(x,y,z) = \sqrt{\sum_j^r\sum_i^k \sigma_{ij}^2\omega_i^2\omega_j^2\varphi_i(x,y,z)\varphi_j(x',y',z')} \tag{7}$$

For high-rise buildings, the combination of the modes of vibration in the two-sway and one-torsional modes is sufficient. However, super high-rise buildings are more flexible because of their height, and thus, high modes and mode coupling may need to be considered. In this paper, a combination of the first 30 modes was used.

The maximum response subject to the fluctuating wind load (deviation from the time average) could be estimated using the following equation: $Y = g \cdot \sigma$, where g is the peak factor and is expressed as shown in Equation (8).

$$g = (2\ln\nu T)^{1/2} + \frac{0.577}{(2\ln\nu T)^{1/2}} \tag{8}$$

where $\nu = \left\{\frac{\int_0^\infty n^2 S_Y(n)d_n}{\int_0^\infty S_Y(n)d_n}\right\}^{1/2}$; ν is the effective frequency; S_Y is the power spectrum of the wind-induced response $Y(t)$; T is the observation time (600 s is adopted here, according to the average time used in the wind-speed measurement at the meteor observatories in China); and 'sign' is the sign function.

5.2. Equivalent static wind load of super high-rise buildings

The inertia force method used to calculate the equivalent static wind load of high-rise buildings was adopted, where the equivalent aim of the inertia force method is the top peak displacement response of super high-rise buildings.

The steps are as follows:

The displacement vibration equation of high-rise buildings subject to wind loads can be derived from Newton's second law[16]

$$[\mathrm{K}]\{w(t)\} = \{p(t)\} - \left([\mathrm{M}]\ddot{w}(t)\} + [\mathrm{C}]\left\{\dot{w}(t)\right)\right. \tag{9}$$

where [K] is the structural stiffness matrix, including the torsion stiffness matrix and translational stiffness matrix; [M] is the mass matrix, including the translational mass and moment of inertia; [C] is the damping matrix; and $\{p(t)\}$ is the wind load, including the horizontal wind forces and torsion moment acting on story i.

DOI: 10.1002/tal

The right side of Equation (9) is called the generalized wind load, and the dynamic structural response can be considered the static structural response subject to the generalized wind load. The generalized wind load is equal to the structural elastic restoring force $\{P_{\text{eq}}\}$:

$$\left\{\tilde{P}_{\text{eq}}\right\} = [\text{K}]\{w(t)\} \tag{10}$$

With the mode superposition method, Equation (10) can be expressed as shown in Equation (11).

$$\left\{\tilde{P}_{\text{eq}}\right\} = [K]\{w(t)\} = [K]\sum_{j=1}^{n}\{\varphi\}_j q_j(t) \tag{11}$$

where $\{\phi\}_j$ and q_j is the vibration mode vector and generalized coordinates of mode j.

The eigenvalue equation of Equation (9) is

$$[\text{K}]\{\varphi\}_j = \omega_j{}^2[\text{M}]\{\varphi\}_j \tag{12}$$

Substitution of Equation (11) into Equation (12) yields

$$\left\{\tilde{P}_{\text{eq}}\right\} = [\text{K}]\sum_{j=1}^{n}\{\varphi\}_j q_j(t) = [\text{M}]\sum_{j=1}^{n}\omega_j{}^2\{\varphi\}_j q_j(t) \tag{13}$$

As shown in Equation (13), the generalized wind load can be expressed as the combination of the inertia force of each mode.

The equivalent static wind load of mode j is

$$\{P_d(z)\}_j = g\omega_j{}^2[\text{M}]\{\varphi\}_j\sigma_j \tag{14}$$

Thus, the equivalent static wind load corresponding to the peak displacement response of high-rise buildings is the weighted combination of the equivalent static wind load of each mode.

$$\{P_d(z)\}_e = \sum_{j=1}^{S} W_j\{P_d(z)\}_j = g\sum_{j=1}^{S} W_j\omega_j{}^2[\text{M}]\{\varphi\}_j\sigma_j \tag{15}$$

where W_j is the weighting factor of $\{P_d(z)\}_j$ and $W_j = \frac{\sigma_{uj}}{\sigma_u}$, where σ_u is the mean square root of the structural peak response to the fluctuating wind load and σ_{uj} is the mean square root of the peak response of mode j.

With the combination of the mean wind load, the total equivalent static wind load can be expressed as follows:

$$\{\hat{p}(z)\} = \{\bar{p}(z)\} + \text{sign}\{\bar{p}(z)\}\{p_d(z)\} = \{\bar{p}(z)\} + \text{sign}\{\bar{p}(z)\}g\sum_{j=1}^{S} W_j\omega_j{}^2[M]\{\varphi\}_j\sigma_j \tag{16}$$

The total torsion moment of the wind load is the vectorial sum of the torsion moment of the mean wind load M_{mean}, the inertia torsion moment M_{torsion} and the mass eccentricity torsion moment M_{ecc}, as shown in Equation (17). The directions of the inertia torsion moment M_{torsion} and the mass eccentricity torsion moment M_{ecc} are the same as those of the torsion moment of the mean wind load M_{mean}.

DOI: 10.1002/tal

$$M = M_{\text{mean}} + M_{\text{torsion}} + M_{\text{ecc}} \tag{17}$$

6. TORSION MOMENT OF SHENZHEN ENERGY CENTER MANSION

6.1. Power spectrum density of the torsion wind load and wind-induced top torsion angle

The time history of the torsion wind load acting on story 30 at a wind direction of 0° was taken as an example to analyze the power spectrum density of the torsion wind load; the power spectrum density of the fluctuating torsion wind load is shown in Figure 6. Figure 6 shows that most of the energy of the fluctuating torsion wind was distributed under 0.4 Hz, and the peak value occurred at 0.155 Hz. The first four modes of the Shenzhen Energy Center mansion are in the high-energy area of the spectra of the torsion wind load. Because the third and fourth modes have torsion vibration shapes, the wind-induced torsion vibration of the building should be examined.

The power density of the wind-induced top torsion angle along a wind direction of 0° is shown in Figure 7. The background response was dominant under 0.4 Hz, whereas the peak resonant values appeared at 3.17 Hz and 4.02 Hz, corresponding to the third and fourth modes of the building, and the proportion of resonant response was larger than that of background response. The aforementioned conclusion has been confirmed by Gen *et al.* (2007). Thus, the third and fourth modes are dominant in the wind-induced torsion response of the Shenzhen Energy Center mansion.

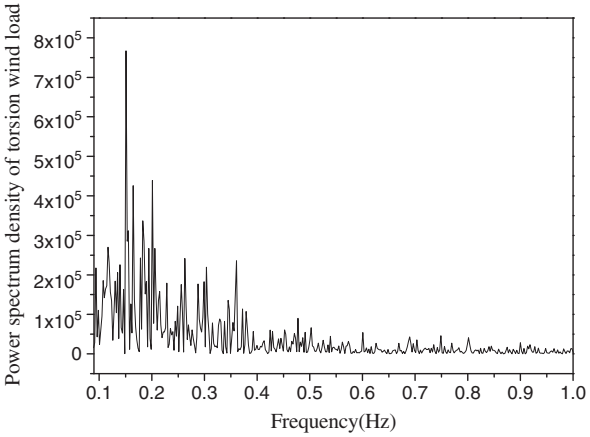

Figure 6. Spectrum of torsion wind load.

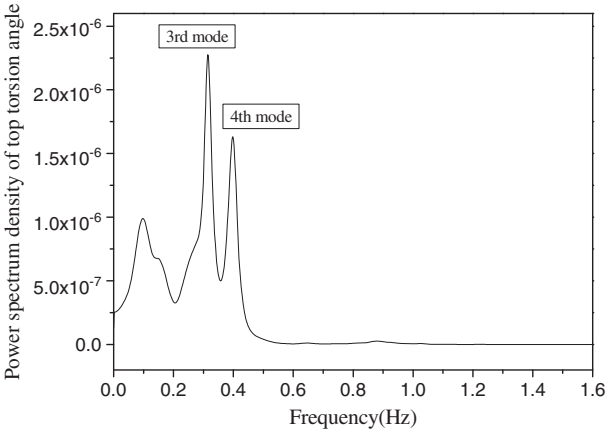

Figure 7. Spectrum of top torsion angle of super high-rise building.

DOI: 10.1002/tal

6.2. *Proportion and eccentricity of three kinds of wind torsion moment*

Wind directions of 0°, 90° and 180° were sampled to analyze the fractions of the mean wind torsion moment, inertia torsion moment and the mass eccentricity torsion moment by caused horizontal inertia forces. The fractions of the mean wind torsion moment, the inertia torsion moment and the mass eccentricity torsion moment caused by horizontal inertia forces, the mass eccentricity, and the eccentricity of the total torsion moment and the radius of gyration are listed in Tables 2–4. The eccentricity of the total

Table 2. The proportions of three kinds of torsion moment and the eccentricity of the torsion moment along 0° wind direction.

	Moment of torsion along 0° wind direction			Eccentricity		Radius of gyration
	Proportion of mean wind torsion moment (%)	Proportion of inertia torsion moment (%)	Proportion of mass eccentricity torsion moment (%)	Torque eccentricity (m)	Mass eccentricity (m)	(m)
Story 43	0.545	0.402	0.053	−2.435	0.743	9.97
Story 42	0.073	0.926	0.001	−3.689	0.096	18.32
Story 41	0.033	0.915	0.052	−3.057	0.979	18.45
Story 40	0.038	0.951	0.011	−2.763	0.08	18.29
Story 39	0.038	0.926	0.036	−2.809	0.491	18.37
Story 38	0.047	0.948	0.005	−2.782	0.153	18.43
Story 37	0.051	0.920	0.030	−2.686	0.257	18.41
Story 36	0.052	0.915	0.032	−2.627	0.258	18.39
Story 35	0.068	0.900	0.033	−2.895	0.276	18.45
Story 34	0.070	0.894	0.036	−2.853	0.306	18.54
Story 33	0.073	0.893	0.034	−2.74	0.323	18.50
Story 32	0.246	0.753	0.001	−3.101	0.51	17.62
Story 31	0.318	0.587	0.094	−2.526	2.088	18.03
Story 30	0.165	0.712	0.124	−2.753	1.269	18.82
Story 29	0.157	0.705	0.138	−2.856	1.423	18.28
Story 28	0.139	0.839	0.022	−3.197	0.489	19.53
Story 27	0.205	0.679	0.116	−2.415	1.111	18.43
Story 26	0.158	0.715	0.127	−2.116	1.083	18.38
Story 25	0.170	0.695	0.135	−2.000	1.093	18.33
Story 24	0.183	0.675	0.143	−1.885	1.114	18.33
Story 23	0.198	0.653	0.149	−1.768	1.093	18.33
Story 22	0.100	0.726	0.174	−1.641	1.091	17.88
Story 21	0.094	0.740	0.166	−1.739	1.167	17.77
Story 20	0.085	0.762	0.153	−1.867	1.01	19.48
Story 19	0.065	0.767	0.168	−1.403	1.02	18.52
Story 18	0.072	0.752	0.176	−1.281	1.02	18.52
Story 17	0.081	0.733	0.186	−1.15	1.02	18.52
Story 16	0.045	0.814	0.141	−1.066	0.815	18.51
Story 15	0.115	0.713	0.172	−0.841	0.867	18.58
Story 14	0.139	0.669	0.192	−0.707	0.887	18.56
Story 13	0.172	0.600	0.228	−0.577	0.947	18.47
Story 12	0.217	0.534	0.249	−0.464	0.912	18.46
Story 11	0.627	0.214	0.159	−0.724	0.909	18.52
Story 10	0.776	0.003	0.221	−0.593	1.131	18.70
Story 9	0.745	0.218	0.037	−0.634	0.67	13.74
Story 8	0.387	0.291	0.323	−2.074	8.475	38.69
Story 7	0.415	0.259	0.326	−1.971	10.546	41.16
Story 6	0.466	0.242	0.293	−1.788	12.203	43.96
Story 5	0.486	0.215	0.299	−1.606	12.619	42.24
Story 4	0.561	0.177	0.261	−1.402	12.705	41.74
Story 3	0.650	0.140	0.210	−1.22	12.335	41.77
Story 2	0.688	0.142	0.170	−0.653	9.107	42.22
Story 1	0.823	0.073	0.105	−0.549	10.495	44.03

DOI: 10.1002/tal

Table 3. The proportions of three kinds of torsion moment and the eccentricity of the torsion moment along 90° wind direction.

	Moment of torsion along 90° wind direction			Eccentricity		Radius of gyration
	Proportion of mean wind torsion moment (%)	Proportion of inertia torsion moment (%)	Proportion of mass eccentricity torsion moment (%)	Torque eccentricity (m)	Mass eccentricity (m)	(m)
Story 43	0.400	0.460	0.140	−0.942	0.743	9.97
Story 42	0.141	0.858	0.001	8.537	0.096	18.32
Story 41	0.157	0.839	0.005	8.574	0.979	18.45
Story 40	0.178	0.818	0.004	7.965	0.08	18.29
Story 39	0.182	0.811	0.007	7.885	0.491	18.37
Story 38	0.185	0.815	0.001	8.072	0.153	18.43
Story 37	0.203	0.788	0.009	7.574	0.257	18.41
Story 36	0.212	0.777	0.011	7.350	0.258	18.39
Story 35	0.183	0.804	0.013	7.538	0.276	18.45
Story 34	0.190	0.795	0.016	7.352	0.306	18.54
Story 33	0.203	0.780	0.017	6.973	0.323	18.50
Story 32	0.138	0.852	0.010	7.009	0.51	17.62
Story 31	0.199	0.710	0.092	5.150	2.088	18.03
Story 30	0.387	0.574	0.039	6.767	1.269	18.82
Story 29	0.354	0.604	0.042	7.313	1.423	18.28
Story 28	0.334	0.666	0	7.686	0.489	19.53
Story 27	0.584	0.367	0.049	4.966	1.111	18.43
Story 26	0.380	0.575	0.046	5.625	1.083	18.38
Story 25	0.426	0.522	0.052	5.110	1.093	18.33
Story 24	0.482	0.459	0.058	4.596	1.114	18.33
Story 23	0.560	0.371	0.069	4.046	1.093	18.33
Story 22	0.498	0.432	0.070	4.257	1.091	17.88
Story 21	0.451	0.491	0.058	4.663	1.167	17.77
Story 20	0.398	0.545	0.057	5.140	1.01	19.48
Story 19	0.501	0.434	0.065	3.633	1.02	18.52
Story 18	0.596	0.331	0.073	3.114	1.02	18.52
Story 17	0.741	0.174	0.084	2.552	1.02	18.52
Story 16	0.910	0.023	0.067	2.041	0.815	18.51
Story 15	0.400	0.472	0.128	1.263	0.867	18.58
Story 14	0.400	0.440	0.160	0.622	0.887	18.56
Story 13	0.600	0.399	0.001	0.015	0.947	18.47
Story 12	0.400	0.386	0.214	−0.567	0.912	18.46
Story 11	0.450	0.461	0.089	−1.523	0.909	18.52
Story 10	0.615	0.314	0.071	−2.186	1.131	18.70
Story 9	0.780	0.195	0.025	−2.660	0.67	13.74
Story 8	0.449	0.461	0.089	8.563	8.475	38.69
Story 7	0.488	0.416	0.096	8.100	10.546	41.16
Story 6	0.535	0.378	0.088	7.579	12.203	43.96
Story 5	0.841	0.126	0.033	14.996	12.619	42.24
Story 4	0.879	0.095	0.026	14.397	12.705	41.74
Story 3	0.913	0.068	0.019	13.885	12.335	41.77
Story 2	0.945	0.045	0.010	12.553	9.107	42.22
Story 1	0.976	0.020	0.004	12.217	10.495	44.03

torsion moment in story *i* is equal to the total torsion moment divided by the horizontal equivalent static wind load in story *i*. Stories 1 through 8 are the podium, and the torsional rigidity and the radius of gyration area are very large.

As shown in Tables 2–4, the mean wind load torsion moment is dominant in the total torsion moment for the low stories because the torsion rigidity of the building is large; in the high stories, the inertia torsion moment is dominant in the total torsion moment because the torsional rigidity of the building is small. The proportion of the torsion moment caused by the mass eccentricity is small;

DOI: 10.1002/tal

Table 4. The proportions of three kinds of torsion moment and the eccentricity of the torsion moment along 180° wind direction.

	Moment of torsion along 180° wind direction			Eccentricity		Radius of gyration
	Proportion of mean wind torsion moment (%)	Proportion of inertia torsion moment (%)	Proportion of mass eccentricity torsion moment (%)	Torque eccentricity (m)	Mass eccentricity (m)	(m)
Story 43	0.285	0.639	0.076	−3.934	0.743	9.97
Story 42	0.128	0.871	0.001	−6.787	0.096	18.32
Story 41	0.124	0.828	0.049	−6.889	0.979	18.45
Story 40	0.127	0.863	0.010	−6.708	0.08	18.29
Story 39	0.127	0.840	0.033	−6.947	0.491	18.37
Story 38	0.128	0.867	0.005	−6.951	0.153	18.43
Story 37	0.130	0.844	0.026	−7.04	0.257	18.41
Story 36	0.130	0.841	0.029	−7.017	0.258	18.39
Story 35	0.137	0.829	0.035	−6.636	0.276	18.45
Story 34	0.138	0.824	0.039	−6.616	0.306	18.54
Story 33	0.140	0.824	0.036	−6.447	0.323	18.50
Story 32	0.142	0.857	0.001	−6.048	0.51	17.62
Story 31	0.161	0.698	0.142	−5.735	2.088	18.03
Story 30	0.128	0.726	0.146	−6.399	1.269	18.82
Story 29	0.127	0.713	0.161	−6.565	1.423	18.28
Story 28	0.123	0.852	0.025	−6.394	0.489	19.53
Story 27	0.138	0.717	0.145	−6.219	1.111	18.43
Story 26	0.110	0.746	0.144	−6.289	1.083	18.38
Story 25	0.111	0.733	0.156	−6.065	1.093	18.33
Story 24	0.112	0.721	0.167	−5.827	1.114	18.33
Story 23	0.113	0.708	0.179	−5.592	1.093	18.33
Story 22	0.106	0.704	0.190	−5.167	1.091	17.88
Story 21	0.105	0.715	0.180	−5.4	1.167	17.77
Story 20	0.105	0.730	0.166	−5.511	1.01	19.48
Story 19	0.070	0.765	0.165	−5.541	1.02	18.52
Story 18	0.178	0.650	0.173	−5.292	1.02	18.52
Story 17	0.188	0.629	0.183	−4.983	1.02	18.52
Story 16	0.097	0.766	0.137	−4.874	0.815	18.51
Story 15	0.192	0.651	0.157	−4.531	0.867	18.58
Story 14	0.229	0.598	0.173	−4.116	0.887	18.56
Story 13	0.279	0.521	0.200	−3.657	0.947	18.47
Story 12	0.343	0.444	0.213	−3.228	0.912	18.46
Story 11	0.357	0.355	0.288	−2.463	0.909	18.52
Story 10	0.556	0.139	0.305	−1.734	1.131	18.70
Story 9	0.496	0.397	0.107	−2.358	0.67	13.74
Story 8	0.411	0.227	0.362	−9.476	8.475	38.69
Story 7	0.451	0.168	0.381	−9.162	10.546	41.16
Story 6	0.524	0.117	0.359	−11.859	12.203	43.96
Story 5	0.662	0.027	0.311	−7.84	12.619	42.24
Story 4	0.654	0.196	0.151	−5.164	12.705	41.74
Story 3	0.514	0.076	0.411	−1.981	12.335	41.77
Story 2	0.236	0.401	0.363	−11.117	9.107	42.22
Story 1	0.403	0.295	0.302	−10.082	10.495	44.03

along a wind direction of 90°, the torsion moment is the largest, and on story 41, the eccentricity caused by the torsion moment is 46% of the radius of gyration of the building, which is much larger than the mass eccentricity. This shows that the torsion moment of the Shenzhen Energy Center mansion caused by the wind load should be considered in the wind-resistant design of the building. Moreover, because the torsion moment caused by the wind load is very sensitive to the wind direction, the torsion moment under different wind directions changes greatly.

DOI: 10.1002/tal

7. CONCLUSIONS

The following conclusions have been drawn from this study.

- The torsion vibration is dominant in the third mode, and the frequency of the third torsion mode is 0.317 Hz, which is close to the frequencies of the first two-sway modes. Because the frequency of the third torsion mode is in the high-energy area of the spectra of the torsion wind load, the wind-induced torsion vibration of the building should be examined.
- The proportion of the resonant response was larger than that of the background response in the wind-induced top torsion angle power density, and the third and fourth modes are dominant in the wind-induced torsion response of the Shenzhen Energy Center mansion.
- In the low stories, where the torsion rigidity of the building is large, the mean wind load torsion moment is dominant in the total torsion moment. In the high stories, where the torsion rigidity of the building is small, the inertia torsion moment is dominant in the total torsion moment. The proportion of the torsion moment caused by the mass eccentricity is small; along the 90° wind direction, the torsion moment is the largest, and on story 41, the eccentricity caused by the torsion moment is 46% of the radius of gyration of the building, which is much larger than the mass eccentricity. Thus, the torsion moment of the Shenzhen Energy Center mansion caused by the wind load should be considered in the wind-resistant design of the building. Moreover, because the torsion moment caused by the wind load is very sensitive to the wind direction, the torsion moment under different wind directions changes greatly.

ACKNOWLEDGEMENTS

This research was financially supported by the National Natural Science Foundation of China under the grant number 50908044, Jiang Su provincial Natural Science Foundation of China under the grant number SBK201123270 and a project funded by the Priority Academic Program Development of Jiangsu Higher Education Institutions.

REFERENCES

Council on Tall Buildings, Structural Branch, Architectural Society of China. 2010. Table of the tall buildings above 180 meters in China mainland. *China Civil Engineering Journal* **43**(5): 104–109.

Irwin PA. 2009. Wind engineering challenges of the new generation of super-tall buildings. *Journal of Wind Engineering and Industrial Aerodynamics* **97**: 328–334.

Kareem A. 1983. Mitigation of wind induced motion of tall building. *Journal of Wind Engineering and Industrial Aerodynamics* **11**: 273–284.

Lam KM, Zhao JG, Leung MYH. 2011. Wind-induced loading and dynamic responses of a row of tall buildings under strong interference. *Journal of Wind Engineering and Industrial Aerodynamics* **99**: 573–583.

Zhang WJ Xu YL, Kwok KCS. 1995. Interference effects on aero-elastic torsional response of structurally asymmetric tall buildings. *Journal of Wind Engineering and Industrial Aerodynamics* **57**: 41–61.

Tallin A, Ellingwood B. 1985. Wind induced lateral–torsional motion of buildings. *Journal of Structural Engineering, ASCE lll* **10**: 2179–2213.

Kareem A. 1985. Lateral–torsional motion of tall buildings to wind loads. *Journal of Structural, ASCE 111* **I 1**: 2479–2496.

Islam MS, Ellingwood B, Corotis RB. 1990. Dynamic response of tall buildings to stochastic wind load. *Journal of Structural Engineering, ASCE 116* **11**: 2982–3002.

Lina N, Letchforda C, Tamurab Y, Liangc B, Nakamura O. 2005. Characteristics of wind forces acting on tall buildings. *Journal of Wind Engineering and Industrial Aerodynamics* **93**: 217–242.

American Society of Civil Engineers (ASCE). 2006. ASCE 7-02 Minimum Design Loads for Buildings and Other Structures, Reston, Va.

China National Standard. 2006. GB50009-2001. Load code for the design of building structures (revised).

Tschanz T, Davenport AG. 1983. The base balance technique for the determination of dynamic wind loads. *Journal of Wind Engineering and Industrial Aerodynamics* **13**: 429–439.

Yip DYN, Flay RGJ. 1995. A new force balance data analysis method for wind response predictions of tall buildings. *Journal of Wind Engineering and Industrial Aerodynamics* **54/55**: 457–471.

Ruo-qiang F. 2008. Research on along-wind and across-wind induced vibration and wind-resist design method of super high-rise building. Postdoctoral pits report of Harbin Institute of Technology.

Cluni F, Gusella V, Spence SMJ, Bartoli G. 2011. Wind action on regular and irregular tall buildings: higher order moment statistical analysis by HFFB and SMPSS measurements. *Journal of Wind Engineering and Industrial Aerodynamics* **99**: 1–9.

Holmes J. 2001. *Wind Loading of Structure*. Spon Press: London.

DOI: 10.1002/tal

Simiu E, Scanlan RH. 1996. *Wind Effects on Structures—An Introduction to Wind Engineering*, 3rd edn. John Wiley & Sons, Inc: New York (USA).

Shuguo L. 1998. Analysis of wind-induced responses for mechanically coupled tall buildings. *Journal of Wuhan University of Hydraulic and Electrical Engineering* **31**(3): 28–34.

Cai J, Pan D-H, Huang Y-S. 2007. Research on torsional vibration control of tall building structures. *Engineering Mechanics* **24**(7): 116–121.

Ge N, Hou H, Zhou X. 2007. Evaluation of Time History Responses of wind Induced torsion vibration on rectangle high rise buildings. *Building Science* **23**(5): 5–10.

AUTHORS' BIOGRAPHIES

Feng Ruo-qiang was born in 1978. He received his doctoral degree from Harbin institute of technology, and now working as an associate professor at the School of Civil Engineering, Southeast University, Nanjing, China. His research focuses on large-span structures, super high-rise buildings and wind engineering. He has published over 40 papers, in which over 20 were cited by SCI or EI.

Ye Jihong was born in 1967. He received her doctoral degree from Tongji University, and now working as a professor at the School of Civil Engineering, Southeast University, Nanjing, China. Her research focuses on seismic performance and wind-induced response of large-span structures. She has published over 70 papers, in which over 50 were cited by SCI or EI.

Guirong Yan was born in 1975. He obtained her PhD from Harbin Institute of Technology in 2006 and served as a post-doctoral research associate at the Polytechnic University of Turin (Italy), Washington University in St. Louis and Purdue University, sequentially. She now works as a lecturer in School of Engineering, University of Western Sydney, Australia. She has research interests primarily in the areas of structural health monitoring and damage detection, sensor technologies and intelligent infrastructures. She has published 36 articles.

Li Qing-xiang was born in 1978. He received his doctoral degree from Zhejiang University, and now working as senior engineer at Guangdong Provincial Academy of Building Research, Guangzhou, China. His research focuses on wind engineering. More than 40 wind tunnel tests of super high-rise buildings and complex special structures have been done by him.

Yao bin was born in 1986. He is pursuing his master's degree in Southeast University.

DOI: 10.1002/tal